Resonant excitation of relativistic-ion cyclotron orbital motion

Shenheng Guan, Michael V. Gorshkov,* George M. Alber, and Alan G. Marshall[†,‡]
Department of Chemistry, 120 West 18th Avenue, The Ohio State University, Columbus, Ohio 43210
(Received 26 June 1992)

A technique is proposed for the excitation of coherent cyclotron motion of ions undergoing a relativistic mass increase. The equations of relativistic-ion cyclotron motion excited by an rf electric dipolar field of fixed peak-to-peak amplitude and a phase that exactly matches the ion cyclotron orbital phase during the excitation process are solved analytically. The resonant cyclotron-motion excitation method is well-suited for bringing ions of low mass-to-charge ratio coherently to a large cyclotron orbital radius for detection or ejection. The method is demonstrated for the excitation of $^{12}C^{3+}$ ions up to about 1% of the speed of light in the cubic ion trap of a Fourier-transform ion cyclotron-resonance mass spectrometer.

PACS number(s): 35.10.Bg, 03.30.+p, 42.50.Vk, 29.20.Hm

I. INTRODUCTION

Precise measurements based on the principle of ion cyclotron resonance (ICR) have provided accurate determination of several important fundamental constants [1–10]. A single ion or a small number of ions are trapped by a uniform static magnetic field and a parallel quadrupolar electrostatic potential. Ion motion in such a trap can be analyzed into three fundamental modes, namely, cyclotron, magnetron, and axial (or trapping) motion [11]. At very low pressure and in the absence of noncollisional relaxation processes, these motions can be considered as independent harmonic oscillators, each with a precisely measurable oscillation frequency. The precision with which a given oscillation frequency can be determined is directly related to the length of time that the oscillation is observed.

For a quadrupolar electrostatic trapping potential, the magnetron frequency is nearly independent of the ionic mass-to-charge ratio m/q, the axial oscillation frequency is inversely proportional to $\sqrt{m/q}$, and the ion cyclotron orbital frequency is inversely proportional to m/q. Thus m/q may be determined from the axial and/or cyclotron orbital frequencies. A near-perfect quadrupolar electrostatic potential requires that the trap surfaces be machined in the shape of hyperboloids of revolution: a "ring" electrode whose central axis is parallel to the magnetic-field direction, and two "end-cap" electrodes (Penning trap). Additional "shim" rings may be added to correct for the nonquadrupolar potential distortion resulting from finite truncation of infinitely extended electrodes [6,12]. The axial motion of a single ion or a small ensemble of ions may then be driven (for example) by an oscillating rf voltage applied to one end-cap electrode, and detected from the image current induced on the other end-cap electrode by the spatially coherent axial motion of ions. Other motional modes may then be detected by means of various methods of coupling those motions to the (detectable) axial motion. Such techniques were developed by Dehmelt and co-workers [11], and have usually been carried out for detection of one or a few ions of a single m/q value.

Alternatively, Fourier-transform ion cyclotron-resonance mass spectrometry (FT-ICR-MS or FTMS) provides multichannel detection capability that allows for the simultaneous detection of ions of a wide range of m/q values [13,14]. In a typical FT-ICR-MS experiment, ions are trapped in an approximately quadrupolar potential produced inside a cubic (or segmented cylindrical) arrangement of electrodes (typically 2.5–5 cm on each side) by applying a constant trapping voltage to each of two opposed trapping electrodes (corresponding to the "end caps" of a Penning trap). A dipolar rf excitation electric field, at the cyclotron frequency of the ion of m/q of interest, is applied differentially between one of the two remaining pairs of opposed sides of the cube, until ions are driven radially outward to an ion cyclotron orbital radius of ~ 1 cm; the image current induced on the remaining pair of electrodes is then converted to a voltage and sampled at equally spaced time increments. This discrete time-domain signal is then subjected to discrete Fourier transformation to produce a frequency-domain spectrum, which is then converted (see below) into an m/q spectrum [15]. The most obvious advantage of single-ion detection is the absence of space-charge effects, which shift the detected ion cyclotron orbital frequency downward. Conversely, the main advantage of the FT-ICR approach for mass difference measurements for closely spaced mass doublets is that ions of both m/q values are present together, so that the systematic error due to magnetic-field drift (the largest systematic error in single-ion trapping experiments) is reduced by a factor of $(m_2-m_1)/m_1$ ($\approx 10^{-5}$ for the $^3H^+$-$^3He^+$ doublet, for example).

A major problem for precise FT-ICR mass measurements of ions of low m/q is the relativistic mass increase during excitation of ion cyclotron motion [16,17]. On the one hand, it is necessary to increase the ion cyclotron orbital radius in order to generate a spatially coherent ion packet that passes sufficiently close to the detector electrodes to produce a measurable image current. On the other hand, a large ICR orbital radius corresponds to

high ion speed, leading to a relativistic increase in ion mass: e.g., $^3He^+$ at an ion cyclotron orbital radius of 1 cm at 7 T reaches a cyclotron orbital velocity that is $\sim 1\%$ of the speed of light! Since the ion cyclotron orbital frequency is approximately inversely proportional to ion mass, a larger ICR orbital radius results in a lower cyclotron frequency: e.g., a proton with an ion cyclotron orbital radius of 1 cm at 7 T is relativistically shifted by 25 kHz below the "rest-mass" cyclotron frequency. This situation is analogous to an anharmonic mechanical oscillator, for which the frequency of oscillation varies with oscillation amplitude [18].

The relativistic frequency shift presents several problems. First, excitation (or radial ejection) of ions of a given m/q by use of fixed-frequency excitation to increase their cyclotron orbital radii becomes difficult, because the ions move out of resonance as soon as their relativistic frequency shift becomes larger than the excitation bandwidth (typically ≤ 1 kHz). Over a sufficiently long excitation period, ions may even decelerate back to their starting point (see Sec. IV). The relativistic shift becomes significant for both singly charged low-mass ions (e.g., $^3He^+$) and for multiply charged heavy atoms (e.g., $^{238}U^{91+}$). The problem was recognized by McMillan as early as 1937 in connection with some of the early cyclotron experiments, but the defocusing effect from an inhomogeneous magnetic field was larger than that from the relativistic frequency shift in the 37-in. Berkeley cyclotron [19]. The relativistic frequency shift for electrons was taken into account in the synchrotron (i.e., frequency-modulated cyclotron) by decreasing the frequency of the applied "dee" voltage with time during the acceleration event (see Sec. IV) [20]. Second, even if the duration of the excitation event is sufficiently short that its frequency-domain bandwidth extends to the relativistically shifted frequency, then the excitation amplitude and phase are independent of frequency, but the ion cyclotron orbital phase lags increasingly behind the excitation phase as the ion gains speed (and thus becomes heavier, with slower ion cyclotron orbital frequency). Thus, ions of slightly different rest mass will be excited to slightly different cyclotron orbital radii by the same excitation wave form. For accurate measurement of the mass difference in a mass doublet, it is essential that both ions in the doublet be excited to exactly the same ion cyclotron orbital radius.

The three most common means for exciting ion cyclotron orbital motion in FT-ICR-MS are (a) fixed-frequency excitation [21] (also known as "impulse" or "burst" excitation), in which ions are accelerated by a short single-frequency rf pulse—fixed-frequency excitation is widely used for precise mass measurements over a narrow m/q range; (b) linear frequency-sweep ("chirp") excitation [22,23], consisting of a sinusoidal rf signal of fixed amplitude and of linearly increasing frequency—chirp excitation is useful for exciting ion cyclotron resonances over a wide m/q range; and (c) stored-wave-form inverse-Fourier-transform (SWIFT) excitation [24,25], in which the excitation wave form is synthesized by inverse Fourier transformation from the specified spectrum—SWIFT excitation is the most general method and is especially useful for selective excitation and/or ejection of ions of several different m/q ranges. All of the methods mentioned above are based on the assumption that the ICR system is linear (detected signal is proportional to excitation amplitude at that frequency) [26,27], and that the ion cyclotron frequencies remain constant throughout the excitation event. Under these conditions, the post-excitation ion cyclotron orbital radius is directly proportional to the excitation spectral magnitude at that frequency. However, for relativistic ions, the ICR response is nonlinear and the ion cyclotron orbital frequency varies with time during the excitation; in that case, one must calculate the ion trajectory directly in order to determine the post excitation ion cyclotron orbital radius.

In this paper, we propose a resonant time-domain excitation wave form whose frequency matches the instantaneous relativistic-ion cyclotron orbital frequency and whose phase matches that of the relativistic-ion cyclotron orbital velocity throughout the excitation process. We begin by deriving a general analytical solution to the equations of relativistic cyclotron motion for arbitrary time-varying electric-field excitation. Under the simplifying condition that the excitation amplitude be held constant, the excitation phase is found to increase quadratically with time. We then compare the behavior of ion cyclotron orbital velocity, position, and frequency during the excitation event in both relativistic and nonrelativistic limits. Theoretical simulations are then compared with experimental FT-ICR results for $^{12}C^{3+}$ at 7.0 T, and good agreement is found.

II. THEORY

A. Equation of relativistic-ion cyclotron motion during excitation

The relativistic equation of motion of a positive ion of charge q, mass m, and velocity $\mathbf{v}$ (and speed $|\mathbf{v}|=v$) moving in a uniform magnetic field $\mathbf{B}=-B\mathbf{k}$ and a quadrupolar trapping field, and driven by an excitation electric field $\mathbf{E}(t)$, can be written in SI *(Système International)* units as [28]

$$\frac{d}{dt}\left[\frac{\mathbf{v}}{\left[1-\frac{v^2}{c^2}\right]^{1/2}}\right]=\omega_+\mathbf{k}\times\mathbf{v}+\frac{q}{m}\mathbf{E}(t)\ . \tag{1}$$

Here the equations of motion have been separated into azimuthal and axial components, and only the cyclotron motion is considered. (The magnetic field is chosen to point in the negative z direction, so that the ion cyclotron frequency is positive for a positive ion.) ω_+ is the reduced cyclotron frequency,

$$\omega_+=\frac{\omega_c}{2}+\frac{\omega_c}{2}\left[1-\frac{2\omega_z^2}{\omega_c^2}\right]^{1/2}=\omega_c-\omega_-\ , \tag{2}$$

in which ω_- is the magnetron frequency, and ω_c is the unperturbed cyclotron angular frequency

$$\omega_c=\frac{qB}{m} \tag{3}$$

of a single ion in the absence of any electric field. For an orthorhombic ion trap, the trapping oscillation frequency ω_z is given by

$$\omega_z = \left[\frac{2\alpha q V_{\rm tr}}{m a^2} \right]^{1/2} , \tag{4}$$

in which α and a are trap geometric factors (e.g., for a cubic trap, $\alpha = 2.773\,73$ and a is the length of one side [27]), and $V_{\rm tr}$ is the trapping voltage applied to each trapping plate. If we now represent the x and y components of the electron field **E** and velocity **v** as the real and imaginary parts of the complex quantities $\mathcal{E}(t)$ and v, we may rewrite Eq. (1) as

$$\frac{d}{dt}\left[\frac{v}{\left[1-\frac{v^2}{c^2}\right]^{1/2}} \right] = i\omega_+ v + \frac{q}{m}\mathcal{E}(t) , \tag{5}$$

in which

$$v = v_x + iv_y = v(t)e^{i\phi(t)} \tag{6}$$

and

$$\mathcal{E}(t) = E_x + iE_y = E_0(t)e^{i\varphi(t)} , \tag{7}$$

where v and ϕ are the amplitude and phase of the ion velocity, and E_0 and φ are the amplitude and phase of the excitation electric field. Equation (5) can be rewritten as

$$\frac{d}{dt}\left[\frac{v}{\left[1-\frac{v^2}{c^2}\right]^{1/2}} \right] + i\frac{v}{\left[1-\frac{v^2}{c^2}\right]^{1/2}}\frac{d\phi}{dt} = i\omega_+ v + \frac{q}{m}E_0(t)e^{i[\varphi(t)-\phi(t)]} . \tag{8}$$

B. Fixed-frequency excitation

In general, the equations of ion motion for fixed-frequency excitation are nonlinear; an analytical solution exists only when $v/c \ll 1$ and ω_+ is time independent. On-resonance excitation has previously been analyzed in this nonrelativistic limit [15,26,27]. For circularly polarized fixed-frequency excitation at angular frequency ω_+,

$$\mathcal{E}(t) = E_0(t)e^{i\omega_+ t} = E_0\cos(\omega_+ t) + iE_0\sin(\omega_+ t) ,$$

and real and imaginary parts of Eq. (8) become

$$\frac{dv}{dt} = \frac{qE_0}{m}\left[1-\frac{v^2}{c^2}\right]^{3/2}\cos[\omega_+ t - \phi(t)] , \tag{9}$$

$$\frac{d\phi(t)}{dt} = \omega_+\left[1-\frac{v^2}{c^2}\right]^{1/2}\left[1+\frac{qE_0}{vm\omega_+}\sin[\omega_+ t - \phi(t)]\right] . \tag{10}$$

The steady-state solution of Eqs. (9) and (10) was first investigated by Kaplan [29]. Experimental results obtained by Gabrielse, Dehmelt, and Kells [30] agree well with the predictions of Kaplan. However, for the FT-ICR experiment, we require the time-dependent ion position and velocity resulting from a finite-duration time-domain excitation wave form. In Sec. II.C, we integrate the differential equations of ion motion numerically to obtain the response to a fixed-frequency excitation.

C. Resonant (phase-modulated) excitation

We seek the solution of Eq. (8) for the case of continuously on-resonance excitation, namely, that the phase of the excitation field follows *exactly* the phase of the ion velocity: $\varphi(t) = \phi(t)$. For that condition, Eq. (8) simplifies to

$$\frac{d}{dt}\left[\frac{v}{\left[1-\frac{v^2}{c^2}\right]^{1/2}} \right] = \frac{q}{m}E_0(t) , \tag{11a}$$

$$\frac{d\phi}{dt} = \omega_+\left[1-\frac{v^2}{c^2}\right]^{1/2} , \tag{11b}$$

$$\varphi(t) = \phi(t) . \tag{11c}$$

Equation (11a) may be solved by direct integration for a specified $E_0(t)$, and the phase function can be obtained by integration of Eq. (11b). Here, however, we seek analytical expressions for both v and ϕ under the additional simplifying condition that the excitation electric-field amplitude is fixed: $E_0(t) = E_0 = \text{const}$. For an ion of zero initial speed, the ion trajectory can then be expressed as

$$v(t) = \frac{\frac{qE_0}{m}t}{\left[1+\left[\frac{qE_0 t}{mc}\right]^2\right]^{1/2}} , \tag{12}$$

$$\phi(t) = \omega_+\frac{mc}{qE_0}\ln\left[\frac{qE_0 t}{mc} + \left[1+\left[\frac{qE_0 t}{mc}\right]^2\right]^{1/2}\right] . \tag{13}$$

In most FT-ICR-MS experiments, $qE_0 t/mc \ll 1$. For example, for a proton resonantly excited for 1 ms by application of 10 $V_{(p\text{-}p)}$ between a pair of infinitely extended electrodes 5 cm apart, $qE_0 t/mc = 0.016\,053$. Equation (13) may therefore be expanded to second order in $qE_0 t/mc$ to give

$$\phi(t) = \omega_+\left[t - \frac{1}{6}\left[\frac{qE_0}{mc}\right]^2 t^3\right] , \tag{14}$$

in which the instantaneous ion cyclotron angular orbital frequency ω' is

$$\omega' = \frac{d\phi(t)}{dt} = \omega_+\left[1-\frac{1}{2}\left[\frac{qE_0 t}{mc}\right]^2\right] . \tag{15}$$

Thus, if the excitation is to be maintained on-resonance with the instantaneous ion cyclotron orbital frequency, then the excitation frequency must decrease quadratically with time, according to Eq. (15). Finally, note that if dipolar excitation of amplitude $E_0(t)$ is used, then E_0 in Eqs. (9)–(15) should be replaced by $E_0(t)/2$; and, of

course, peak-to-peak rf voltage should be divided by 2 to obtain the rf voltage amplitude from which $E_0(t)$ is obtained.

III. EXPERIMENT

All experiments were carried out on a home-built FT-ICR mass spectrometer [31] consisting of a 7.0446-T 150-mm-bore-diam superconducting solenoidal magnet (Oxford Instruments, England), a high-vacuum system with ten 300-L/s ion pumps and four titanium sublimation pumps (Perkin-Elmer TNB-X), and an Extrel FTMS-2000 computer data station for control of the experimental event sequence as well as visualization, processing, and storage of mass spectral data.

The rf carrier frequency for ion cyclotron excitation was produced by a PTS-160 frequency synthesizer (100-kHz–160-MHz frequency range). In the fixed-frequency excitation mode, the carrier was gated by a rectangular pulse of adjustable duration from the data station. For resonant dipolar excitation, the following time-domain wave form was used:

$$E(t)=E_0\cos[(\omega_+ t-\beta t^3)] , \tag{16}$$

in which $\beta=\omega_+ q^2E_0^2t^2/6m^2c^2$. To produce this wave form, a carrier signal at ω_{carrier} from the PTS-160 synthesizer was mixed with the following wave form:

$$V(t)=V_0\cos[(\omega_{\text{offset}}t-\beta t^3)] , \tag{17}$$

which was loaded into a home-built SWIFT module interfaced to the Extrel 2000 data station. $\nu_{\text{offset}}=\omega_{\text{offset}}/2\pi$ was chosen to be 100 kHz. After mixing, the final excitation signal contains two frequency components (see Fig. 1). Only the component with initial frequency, $\omega_{\text{carrier}}-\omega_{\text{offset}}=\omega_+$, is effective in exciting ion cyclotron orbital motion, because that component exactly tracks the ion cyclotron orbital frequency as it decreases during the excitation process. Since the relativistic frequency shift in our experiments is less than 2 kHz, a large value of ω_{offset} effectively prevents interference from the other off-resonance component resulting from the mixing procedure. The signal after mixing was amplified and applied differentially (i.e., azimuthal dipolar excitation to the excitation electrode plates of a 2-in. cubic ICR ion trap). The transient time-domain signal obtained by differential dipolar detection from the pair of plates orthogonal to the first pair was amplified and mixed with a reference sinusoidal signal from another (PTS-40) rf frequency synthesizer.

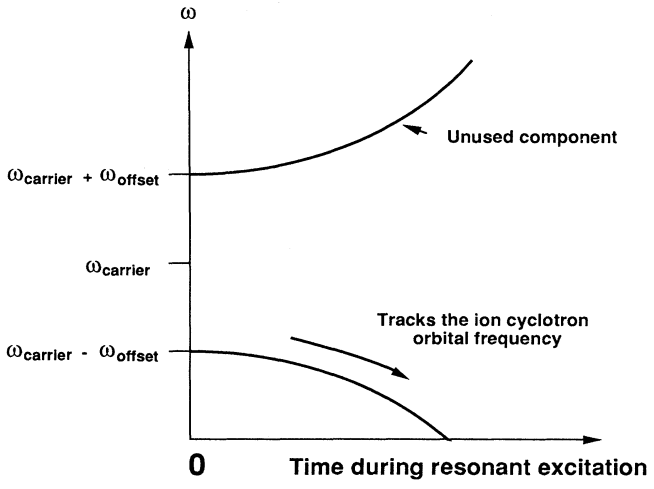

FIG. 1. Schematic diagram of the frequencies of two signal components obtained by mixing a fixed sinusoidal carrier signal with a sinusoid of fixed amplitude and quadratically increasing phase, as a function of time during the excitation event. The component seen in the lower curve is used to excite resonant relativistic-ion cyclotron motion. Interference from the unwanted component shown in the upper curve is reduced by offsetting the carrier frequency by ω_{offset} from the initial ("rest-mass") ICR orbital frequency.

$^{12}C^{3+}$ ions were formed by electron-impact ionization (85-eV electron beam for 5–20 s at an emission current of 3.0 μA at 4×10^{-11} Torr of CH_4). Unwanted ions, CH_4^+, CH_3^+, CH_2^+, CH^+, C^+, and C^{2+} generated by electron ionization generate a space charge distributed along the central z axis of the trap and shift the ion cyclotron orbital frequencies of rf-excited ions, thereby complicating the determination of ω_+. Unwanted ions were therefore ejected in the z direction (i.e., the magnetic-field direction) by applying an rf frequency-sweep ("chirp") to one trapping electrode of the ICR trap [32], such that the "chirp" frequency range spanned the range of trapping frequencies [see Eq. (2)] of the unwanted ions.

Ions were excited and detected by the use of a standard FT-ICR experimental event sequence: quench period of 10 ms; ion formation as described above; ejection of unwanted ions; excitation of cyclotron motion of ions followed by a ~50-ms delay; data acquisition (8-K time-domain data points, 2-kHz frequency bandwidth, 4-kHz sampling rate). The digitized time-domain data were then subjected to a fast Fourier transform and displayed in magnitude mode.

IV. RESULTS AND DISCUSSION

A. Fixed-frequency excitation

Figure 2 shows the relativistic instantaneous ion cyclotron orbital frequency for C^{3+} ions during the excitation event. The frequency of the excitation was fixed at the ion cyclotron orbital frequency of ions at rest ($\nu_+=\omega_+/2\pi$, the rest-mass cyclotron frequency). Initially, the ion cyclotron orbital velocity is in phase with the resonant-frequency rf electric excitation field: $\varphi(0)=\phi(0)$. As ions absorb energy and accelerate during excitation, their relativistic mass increases, their ion cyclotron orbital frequency decreases [see Eq. (15)], and the phase of the ion velocity periodically oscillates in and out of phase with respect to the driving electric field, leading to periodic deceleration and reacceleration of the ions. The solid curve in Fig. 2 was obtained by numerical integration of Eqs. (7) and (8), showing excellent agreement with the experimental data points in the same figure. The ion cyclotron orbital radius r is related to the relativistic frequency shift, $\nu_+(\text{rest})-\nu_+(\text{relativistic})$, by the following equation to first order in $(v/c)^2$ [16,17]:

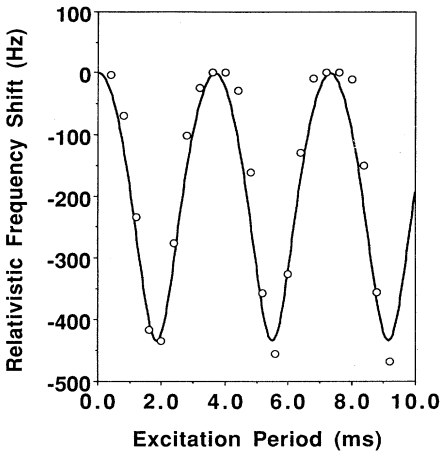

FIG. 2. Relativistic-ion cyclotron orbital frequency shift for $^{12}C^{3+}$ ions at 7.004 46 T resulting from an increase in ion speed during fixed-frequency excitation ($12V_{(p\text{-}p)}$, 62.5 V/m, $\nu_+ = 27.049\,08$ MHz, trapping potential equal to 5 V across a 2 in. cubic trap) at the "rest-mass" ion cyclotron orbital frequency. Note the oscillating frequency shift resulting from the accumulated phase difference between the excitation field and the ion cyclotron orbital velocity.

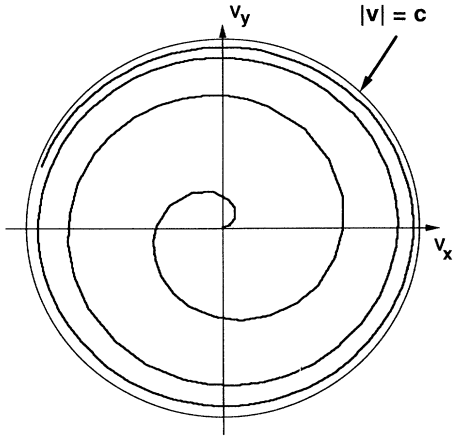

FIG. 3. Positive-ion cyclotron velocity trajectory (magnetic field directed into the plane of the paper) during resonant excitation. For a relativistic ion, the ion acceleration decreases as the ion approaches the speed of light (i.e., the circle at $v = c$). In contrast, a nonrelativistic ion (not shown) undergoes constant acceleration during resonant excitation.

$$\nu_+(\text{relativistic}) = \nu_+(\text{rest}) - \frac{2\pi^2\nu_+^3 r^2}{c^2} , \tag{18a}$$

or, equivalently,

$$r = \left[\frac{c^2[\nu_+(\text{rest}) - \nu_+(\text{relativistic})]}{2\pi^2\nu_+^3} \right]^{1/2} . \tag{18b}$$

Thus, ions are periodically excited to larger cyclotron orbital radius and then deexcited back to the origin, an effect qualitatively similar to that of off-resonance fixed-frequency excitation [33]. Fixed-frequency excitation therefore cannot be used to drive relativistic ions continuously outward to ever-larger cyclotron orbital radius.

B. Resonant (phase-modulation) excitation

The effect of resonant cyclotron excitation of a relativistic ion can be illustrated in several ways. The relativistic-ion trajectory derived from Eqs. (12) and (13) for resonant cyclotron excitation is illustrated in two-dimensional velocity space in Fig. 3. Time integration of the velocity trajectory leads to the ion trajectory for resonant cyclotron excitation, viewed in Cartesian position space, shown in Fig. 4. The ion cyclotron orbital *radius* grows continuously, even for a relativistic ion. For a nonrelativistic ion, m is approximately constant and v increases linearly with time, so that r also increases linearly with time during resonant excitation. However, at relativistic speed (see Fig. 5), ion cyclotron orbital *velocity* at first increases linearly with time and then more gradually as the ion approaches light speed, whereas ion mass increases faster than linearly with time, such that the product mv (and thus the ion cyclotron orbital radius $r = mv/qB$) increases faster than linearly with time during resonant excitation. The instantaneous ion cyclotron orbital *frequency* initially decreases quadratically with time during resonant excitation, changing to a lower rate of decrease toward zero frequency as the ion approaches light speed (see Fig. 6).

For low-mass charged atoms, Eq. (15) provides a good approximation to the relativistic frequency shift, which is on the order of 10^3 parts per million (ppm) or less for an ion cyclotron orbital radius of ≤ 1 cm at 7 T. The magnitude-mode Fourier-transform spectrum of the quadratic frequency-sweep time-domain resonant excita-

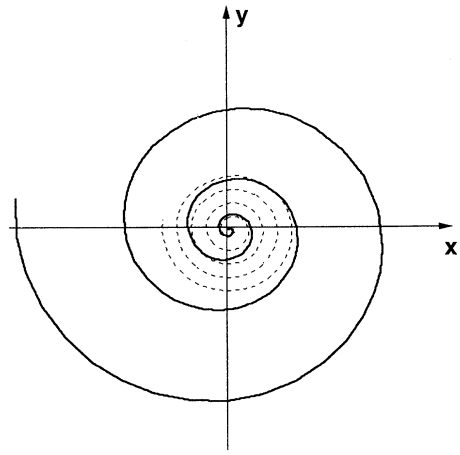

FIG. 4. Positive-ion cyclotron orbital position trajectory (solid curve) corresponding to the velocity trajectory shown in Fig. 3. The ion cyclotron orbital radius increases continuously at an increasing rate during resonant excitation under the excitation condition. The ion cyclotron orbital radius of a nonrelativistic ion (i.e., $c \rightarrow \infty$) increases at a constant rate during resonant excitation (dashed curve).

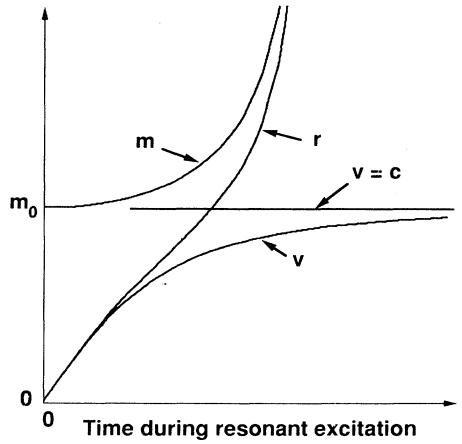

FIG. 5. Positive-ion relativistic mass, cyclotron orbital velocity, and relative ion cyclotron orbital radius as a function of time during resonant excitation. This plot accounts for the relativistic-ion position trajectory of Fig. 4 (see text).

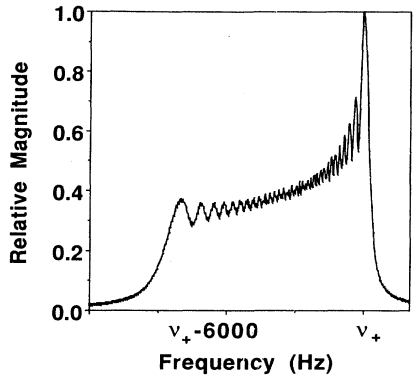

FIG. 7. Magnitude spectrum (scaled to the maximum magnitude) obtained by Fourier transformation of a time-domain undamped sinusoid of fixed amplitude and quadratically increasing phase. $\nu_+ = 27.049\,08$ MHz is the "rest-mass" ion cyclotron orbital frequency (i.e., the initial frequency for resonant excitation). Other parameters as in Fig. 2.

tion wave form of Eq. (16) for resonant cyclotron excitation of $^{12}C^{3+}$ ions, as calculated from Eq. (16), is shown in Fig. 7. Although the time-domain wave-form amplitude is constant during the excitation event, the nonlinear frequency sweep results in a spectrum described by a Fresnel function, with nonuniform magnitude as a function of frequency.

An experimental test of the proposed resonant excitation is provided by Fig. 8, which shows the relativistic-ion orbital frequency shift as a function of time during resonant dipolar excitation. The solid curve is the theoretical frequency shift, which varies quadratically with time during resonant excitation. A much larger relativistic frequency shift was achieved than with fixed-frequency excitation, because resonant excitation drives the ions to much larger cyclotron orbital radii. For example, with fixed-frequency excitation, we were unable to excite $^{12}C^{3+}$ ions to an ion cyclotron orbit corresponding to a relativistic frequency shift greater than 500 Hz (i.e., an ion cyclotron orbital radius greater than ~ 1 cm), whereas resonant excitation readily produced a frequency shift of 1.4 kHz (1.7-cm ICR orbital radius). The experimental data in Fig. 8 agree nicely with the theoretical curve. The data of Fig. 8 do not extend out to the less-than-quadratic behavior of Fig. 5, because ions are radially ejected from our trap before they reach such large cyclotron orbital velocity [34]. Moreover, we found that the final ion cyclotron orbital radius depended strongly on the choice of initial excitation frequency. Ideally, the initial excitation frequency should correspond to the rest-mass ion cyclotron orbital frequency ω_+, but space charge at the center of the trap can lower the ion cyclotron orbital frequency somewhat [16,17]. The effect of space charge from ions at the center of the trap decreases with increasing ion cyclotron orbital radius, as seen by

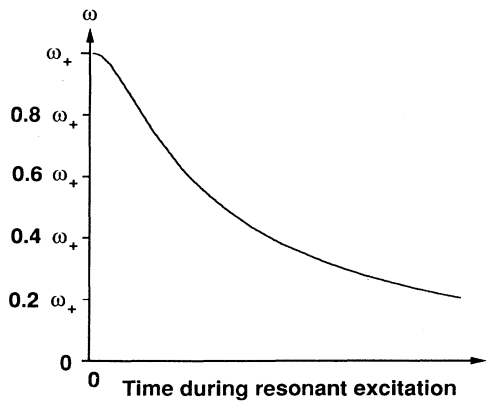

FIG. 6. Reduced ion cyclotron orbital frequency as a function of time during a resonant excitation event. The ICR orbital frequency initially decreases quadratically with time, and then approaches zero asymptotically. Other parameters as in Fig. 2.

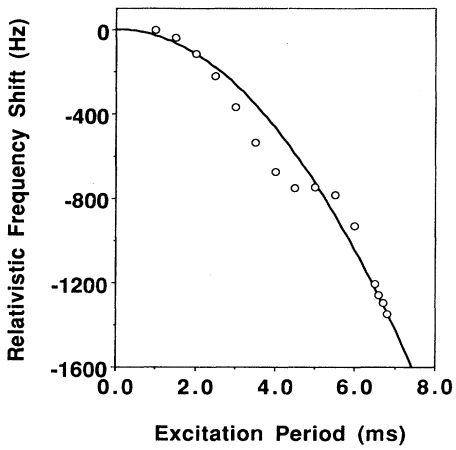

FIG. 8. Theoretical (solid curve) and experimental (open circles) relativistic shift in ion cyclotron orbital frequency of $^{12}C^{3+}$ ions at 7.0446 T as a function of time during resonant excitation. Other parameters as in Fig. 2. The theoretical curve was obtained by evaluating $d\phi(t)/dt$ from Eq. (13) for dipolar excitation.

the closer agreement between theory and experiment for larger ICR orbital radius in Fig. 8. Finally, it should be noted that space-charge effects, nonquadrupolar trapping potential, and spatially nonuniform rf excitation field can also shift the ion cyclotron orbital frequency; these systematic shifts can be determined by analyzing an experiment conducted at a series of values of ICR orbital radius, trapping voltage, and number of ions, as will be described in detail elsewhere. For ions of $m/z \leq 10$ or so, at 7 T, the relativistic shift is the largest.

Finally, we should comment on differences between frequency modulation in the synchrotron and the present ion cyclotron. In the synchrotron, the "dee" voltage of constant amplitude is switched in polarity twice per revolution of an electron (or other relativistic-speed charged particle); thus, the "capture efficiency" of the synchrotron depends strongly on the relative phase of the ion cyclotron motion and the switching time, so that the "dee" voltage has the correct sign as the ion reaches the space between the "dees" [20]. In contrast, the present excitation is continuous (rather than pulsed) and sinusoidal (rather than square-wave), and the initial ion cyclotron radius is much smaller (≤ 0.1 mm) than the post excitation cyclotron radius (~ 1 cm); under these conditions, ions become spatially coherent within a few cycles of the cyclotron frequency, independent of initial ion cyclotron phase [33]. Thus, phase matching of excitation and ion cyclotron motion is not a problem in ICR experiments.

V. CONCLUSIONS AND FUTURE DIRECTIONS

We have derived an analytical solution for the equations of relativistic-ion cyclotron motion. If the excitation phase exactly matches the ion cyclotron orbital velocity phase, the equations can be directly integrated for a specified resonant excitation. For resonant excitation at fixed amplitude, simple analytical expressions for ion speed and cyclotron orbital phase can be obtained. The exact phase of the required electric excitation field for ions that experience a relativistic shift of any magnitude is given by Eq. (13), which can be approximated by Eq. (14) for most ICR experiments. Experimental implementation of the excitation method is achieved by mixing the appropriate wave form from an arbitrary wave-form generator with a sinusoidal rf carrier signal to reach the appropriate ICR orbital frequency.

The response of $^{12}C^{3+}$ ions to the fixed-frequency excitation and the newly developed resonant excitation signals has been investigated. Simulated and experimental results show a periodic shift in instantaneous ion cyclotron orbital frequency and radius during fixed-frequency excitation. Resonant excitation produces a quadratic decrease in the ion cyclotron frequency with time, as predicted from the theory. The method developed in this paper allows one to obtain large ion cyclotron radii, and thus large kinetic energy for ions of small mass-to-charge ratio in a high static magnetic field. The present method may also be used for highly selective and efficient radial ejection of low-mass ions (e.g., $^4He^+$ in gas chromatograph FT-ICR mass spectrometry.) High-energy ion-neutral collisions, or even some nuclear reactions, in the ion trap of an FT-ICR spectrometer become accessible by the present method. Indeed, the kinetic energy of a proton at 7 T at an ion cyclotron orbital radius of only 2 cm is ~ 1 MeV, and is ~ 2 GeV for an electron.

ACKNOWLEDGMENTS

This work was supported by the National Science Foundation (CHE-9021058) and The Ohio State University.

*Permanent address: Institute of Energy Problems of Chemical Physics, Academy of Science, Moscow 117829, Russia.

†Also at Department of Biochemistry, The Ohio State University, Columbus, OH 43210.

‡Author to whom correspondence may be addressed.

[1] G. Graff, H. Kalinowsky, and J. Traut, Z. Phys. A **297**, 35 (1980).

[2] R. S. Van Dyck Jr. and P. B. Schwinberg, Phys. Rev. Lett. **47**, 395 (1981).

[3] E. N. Nikolaev, Y. I. Neronov, M. V. Gorshov, and V. L. Talrose, Pis'ma Zh. Eksp. Teor. Fiz. **39**, 441 (1984) [JETP Lett. **39**, 534 (1984)].

[4] M. V. Gorshkov, Y. I. Neronov, E. N. Nikolaev, V. L. Tal'roze, and Y. V. Tarbeev (unpublished).

[5] R. S. Van Dyck Jr., P. B. Schwinberg, and H. G. Dehmelt, Phys. Rev. D **34**, 722 (1986).

[6] E. A. Cornell, R. M. Weisskoff, K. R. Boyce, R. W. Flanagan, Jr., G. P. Lafyatis, and D. E. Pritchard, Phys. Rev. Lett. **63**, 1674 (1989).

[7] G. Gabrielse, X. Fei, L. A. Orozco, R. L. Tjoelker, J. Haas, H. Kalinowsky, T. A. Trainor, and W. Kells, Phys. Rev. Lett. **65**, 1317 (1990).

[8] C. Gerz, D. Wilsdorf, and G. Werth, Z. Phys. D **17**, 119 (1990).

[9] J. T. Meek, W. G. Millen, G. W. Stockton, and R. T. Kouzes, Phys. Rev. C **41**, 2921 (1990).

[10] R. S. Van Dyck, Jr., D. L. Farnham, and P. B. Schwinberg, J. Mod. Opt. **39**, 243 (1992).

[11] D. J. Wineland, P. Ekstrom, and H. G. Dehmelt, Phys. Rev. Lett. **31**, 1279 (1973).

[12] R. S. Van Dyck, Jr., F. L. Moore, D. L. Farnham, and P. B. Schwinberg, Phys. Rev. A **40**, 6308 (1989).

[13] A. G. Marshall and P. B. Grosshans, Anal. Chem. **63**, 215 (1991).

[14] A. G. Marshall and L. Schweikhard, Int. J. Mass Spectrom. Ion Proc. **118/119**, 37 (1992).

[15] A. G. Marshall and F. R. Verdun, *Fourier Transforms in NMR, Optical, and Mass Spectrometry: A User's Handbook* (Elsevier, Amsterdam, 1990).

[16] V. L. Talrose and E. N. Nikolaev, Adv. Mass Spectrom. A **10**, 343 (1985).

[17] M. V. Gorshkov, Ph.D. thesis, Moscow Institute of Physics and Technology, 1987.

[18] L. D. Landau and E. M. Lifschitz, *Mechanics* (Pergamon, Oxford; Addison-Wesley, Reading, MA, 1969), Chap. 5,

Sec. 28.
[19] J. L. Heilbron and R. W. Seidel, *Lawrence and His Laboratory: A History of the Lawrence Berkeley Laboratory* (University of California Press, Berkeley, CA, 1989), Vol. 1.
[20] D. Bohm and L. L. Foldy, Phys. Rev. **72**, 649 (1947).
[21] M. B. Comisarow and A. G. Marshall, Chem. Phys. Lett. **25**, 282 (1974).
[22] M. B. Comisarow and A. G. Marshall, Chem. Phys. Lett. **26**, 489 (1974).
[23] A. G. Marshall and D. C. Roe, J. Chem. Phys. **73**, 1581 (1980).
[24] A. G. Marshall, T.-C. L. Wang, and T. L. Ricca, J. Am. Chem. Soc. **107**, 7893 (1985).
[25] A. G. Marshall, T.-C. L. Wang, L. Chen, and T. L. Ricca, Am. Chem. Soc. Symp. Ser. **359**, 21 (1987).
[26] S. Guan, J. Am. Soc. Mass Spectrom. **2**, 483 (1991).
[27] P. B. Grosshans and A. G. Marshall, Anal. Chem. **63**, 2057 (1991).
[28] L. S. Brown and G. Gabrielse, Rev. Mod. Phys. **58**, 233 (1986).
[29] A. E. Kaplan, Phys. Rev. Lett. **48**, 138 (1982).
[30] G. Gabrielse, H. Dehmelt, and W. Kells, Phys. Rev. Lett. **54**, 537 (1985).
[31] N. C. Hill, G. M. Alber, L. Schweikhard, T. L. Ricca, and A. G. Marshall, in *Proceedings of the 39th American Society of Mass Spectrometry Conference on Mass Spectrometry and Allied Topics* (American Society of Mass Spectrometry, Nashville, TN, 1991), p. 1501.
[32] R. T. McIver Jr., in *Lecture Notes in Chemistry Vol. 7,* edited by H. Hartmann and K.-P. Wanczek (Springer-Verlag, Berlin, 1978).
[33] M. Wang and A. G. Marshall, Int. J. Mass Spectrom. Ion Proc. **100**, 323 (1990).
[34] P. Kofel, M. Allemann, H. Kellerhals, and K.-P. Wanczek, Int. J. Mass Spectrom. Ion Proc. **74**, 1 (1986).